Lim et al. *NPG Asia Materials* (2023) 15:7
https://doi.org/10.1038/s41427-023-00464-1

NPG Asia Materials

ARTICLE Open Access

Hybrid graphene electrode for the diagnosis and treatment of epilepsy in free-moving animal models

Jeongsik Lim[1], Sangwon Lee[2,3], Jejung Kim[1], Jeonghoon Hong[4], Sooho Lim[2,3], Kyungtae Kim[2], Jeongwoo Kim[4], Sungchil Yang[5], Sunggu Yang[2,3] and Jong-Hyun Ahn[1]

Abstract

Various electrophysiological and imaging techniques have been studied for the diagnosis and treatment of epilepsy. In particular, electrocorticography (ECoG) provides valuable information that can guide clinical treatment of patients with epilepsy. Currently, it is necessary to define the clinical benefits of ECoG in free-moving animals for the treatment of epilepsy. Here, we present the results of simultaneous recordings of multiple cortical sites and responsive neurostimulations for epilepsy treatment carried out in free-moving rats. In this study, we developed a high-density, flexible electrode array comprising graphene/Au/graphene that stably wraps onto the cortex surface of a living rat brain, exhibiting a superior signal-to-noise ratio. The hybrid graphene multichannel electrode successfully detected brain signals with high-throughput spatiotemporal resolution and substantially suppressed pilocarpine-induced epileptic discharges and behavior. Simultaneous recording and neurostimulation in awake animals can lead to a fundamental change in the treatment of medically intractable epilepsy.

Introduction

Epilepsy is a neurological disorder caused by aberrant dynamism of neural networks, which often leads to spontaneous and recurrent seizure activity[1,2]. Suppressive therapies such as those involving medicines are available; however, a comprehensive cure for the disease has not yet been reported. In particular, the monitoring of epilepsy is important for early remediation and prevention. As such, timely monitoring and treatment of epilepsy can prevent uncontrolled movements, memory loss, and casualties, thereby decreasing morbidity. Therefore, novel neurologic monitoring and diagnostic technologies need to be developed.

Among the various methods for monitoring brain function in patients with epilepsy, electrocorticography (ECoG) measurement is considered the most efficient. Needle-shaped penetrating electrodes implanted deep into the cerebral cortex have generally been used for the detection of ECoG signals and electrotherapy[3–5]. However, these electrodes can induce tissue damage and have limitations in the mapping of functional areas and long-term implantation. As an alternative, surface electrodes that are placed directly on the surface of the cortex have been recently developed. Flexible surface electrodes with significant spatiotemporal resolution permit gap-free integration with the curvilinear surface of the brain, offering a less invasive option for diagnosis and treatment. As a representative demonstration, Malliaras et al. developed a flexible PEDOT:PSS microelectrode array, which can perform very high-resolution recordings of action potentials from the surface of the brain cortex even without penetrating the brain tissue, as was demonstrated in both rats and humans[6,7]. This high-density configuration enabled unprecedented recordings of

Correspondence: Sungchil Yang (sungchil.yang@cityu.edu.hk) or Sunggu Yang (sungguyang@inu.ac.kr) or Jong-Hyun Ahn (ahnj@yonsei.ac.kr)
[1]School of Electrical & Electronic Engineering, Yonsei University, Seoul 03722, Republic of Korea
[2]Department of Nano-bioengineering, Incheon National University, Incheon 22012, Republic of Korea
Full list of author information is available at the end of the article
These authors contributed equally: Jeongsik Lim, Sangwon Lee.

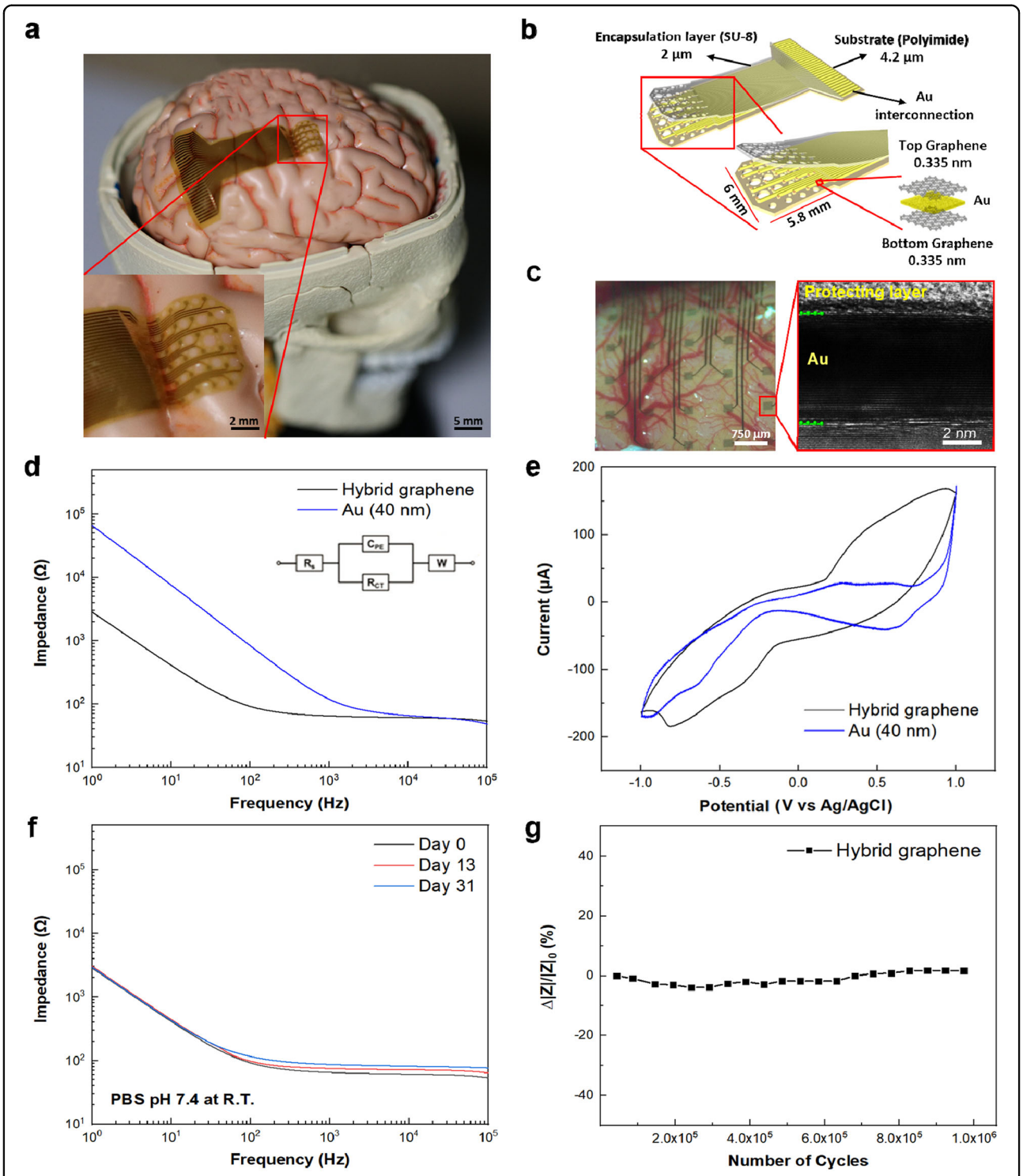

Fig. 1 Multichannel hybrid graphene electrode array to monitor brain activity and electrochemical characterization. a Photograph of the 32-channel hybrid graphene (Gr/Au/Gr) electrode array on an artificial model of the cortex. **b** Schematic illustration of device fabrication. **c** Photograph of a device on the rat brain (left) and TEM image of the hybrid graphene-like thin film used in the electrode array (right). **d** Electrochemical impedance spectroscopy (EIS) of the hybrid graphene electrode and Au (40 nm) electrode for a 1×1 cm^2 area in PBS and the equivalent circuit model fitted with the EIS measurement results. The hybrid graphene electrode shows lower impedance. **e** Cyclic voltammetry results of both electrodes with a scan rate of 200 mV/s. **f** Long-term stability and **g** relative impedance with the cyclic electrical stimulation test of the hybrid graphene electrode.

electrical activity in rat brains, along with good biocompatibility and flexibility. The developed ECoG electrodes were also able to record signals resembling epileptic spikes in a high-fidelity manner. Rogers et al. successfully fabricated even denser and more flexible surface electrode arrays that could record action potentials in various cortical areas[8–11]. However, these advances have thus far been limited to demonstrating simultaneous monitoring and treatment via electric stimulation through a free-moving animal model.

Here, we aimed to demonstrate a highly conformal array of hybrid graphene–Au electrodes to monitor brain activity and relieve epilepsy via electrical stimulation during in-place switching. These electrodes consist of three layers of graphene/Au film/graphene, a material termed "hybrid graphene," which shows low impedance in the frequency bands of brain activities and provides a superior signal-to-noise ratio (SNR) compared with other previous products reported in the literature. Such properties of the electrode array enable both clearer detection of high-spatial resolution local field potentials (LFPs) from the cortical surface and electrical stimulation for alleviating epileptic seizures. In addition, we developed an awake, free-moving mouse model mimicking humans experiencing epilepsy. Here, we showed that graphene-based electrical stimulation using our newly fabricated hybrid graphene multichannel electrodes efficiently controls the behavioral signs of epileptic seizures.

Results

Design and characteristics of the hybrid graphene electrode array

A 32-channel electrode array of graphene (~0.33 nm)/Au (~6 nm)/graphene (~0.33 nm) hybrid structure with ultrathin Au was designed on a flexible polyimide (PI) substrate (~4.2 μm) using a sequence of processes, including transferring the chemical vapor deposition (CVD)-grown graphene to the PI substrate, sputtering Au, and patterning the electrodes (Fig. 1a, b). Atomically thin graphene, which has outstanding mechanical and electrical properties and biocompatibility, forms a good interface with desirable conformal contact with the cortex surface[12–15]. Moreover, the ultrathin Au layer between the two graphene layers effectively reduced the impedance due to its high electrical conductivity. Au film with a minimum thickness of 6 nm was used to facilitate the use of a graphene electrode that forms a good interface and conformal contact with the brain cortex. The hybrid graphene electrode array, which is composed of $250 \times 250\ \mu m^2$ electrodes placed with a pitch of 1000 μm and a total device thickness of ~6.2 μm, presented good mechanical flexibility, low noise level, and high optical transmittance. The electrode array was designed for real-time brain signal measurements and electrical stimulation for epilepsy treatment. In addition, the unique flexibility and thru-holes of the hybrid graphene electrode enabled a desirable uniform surface topography on the brain cortex under severe deformations (Fig. 1c). The high transparency of the substrate and electrode also allows the visual identification of blood vessels on the brain surface. The transmission electron microscopy (TEM) image of the hybrid graphene electrode shows a decently stacked structure of the graphene/Au/graphene layers.

Low impedance can reduce electrical noise and enhance electrical signals in the brain[16,17]. To compare the characteristics of the hybrid graphene and Au electrodes (thickness: ~40 nm), we measured the impedance of both electrodes at different frequencies. The impedance of both electrodes decreased as the frequency increased at low frequencies and saturated at high frequencies. The hybrid graphene electrode exhibited a lower impedance (91.90 Ω) than the Au electrode (839.57 Ω at 100 Hz) (Fig. 1d). Because LFPs have frequencies in the range of 1–100 Hz, the low-impedance hybrid electrode in the low-frequency range measures signals more accurately than Au electrodes. In the optical transmission measurements in the visible region, the hybrid graphene electrode showed 70.4% transmittance, whereas the Au electrode showed only 5% transmittance (Supplementary Fig. 1). This high transmittance of the hybrid electrode allows precise placement of the device at the desired location of the brain surface as well as direct observation of the blood vessels on the brain surface for neural recording. Cyclic voltammetry (CV) measurements were performed to investigate the charge-transfer capacity of both electrodes. The hybrid graphene electrode had a charge storage capacity of $1.65\ mC{\cdot}cm^{-2}$, while the Au electrode exhibited a low value of $0.906\ mC{\cdot}cm^{-2}$ (Fig. 1e and Supplementary Table 1). The high charge storage capacity of the hybrid electrode indicates that it can improve the efficiency of charge transfer in neural stimulation[18] compared with the Au electrode.

To confirm the long-term stability of the hybrid electrodes, we measured the impedance in phosphate-buffered saline (PBS) at physiological pH (7.4) after 31 days and observed a delicate change in the specific frequency range of 15–25 Hz in which epileptic discharges are generally detected (Supplementary Fig. 2). Furthermore, the hybrid electrodes exhibited a negligible degradation of 6.69% after 31 days (Fig. 1f). The relative impedance during repeated electrical stimulation ($>9 \times 10^5$) showed a small change of 4%, indicating that the hybrid graphene can be stably operated even over long-term use (Fig. 1g).

Interface properties of the hybrid graphene electrode

To understand the superior electrical conduction efficiency of Au/graphene electrodes compared to Au

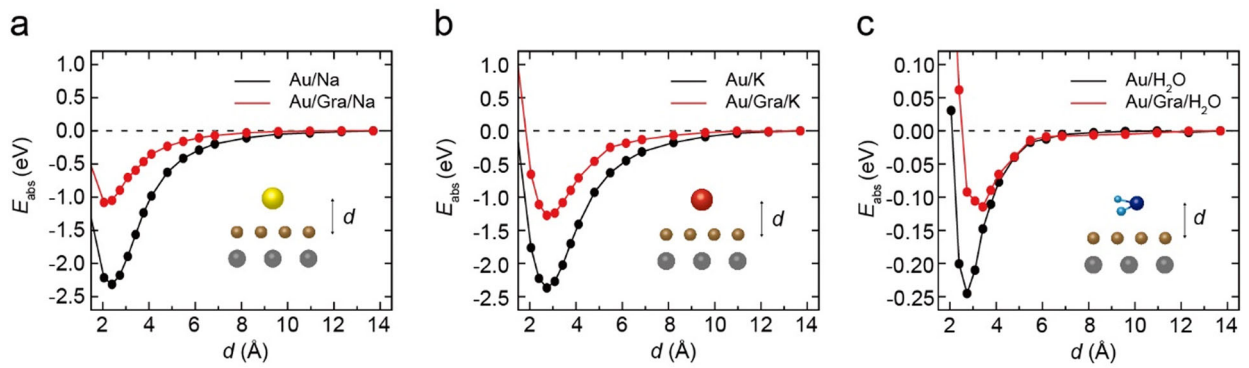

Fig. 2 The effect of graphene on the absorption energy of adsorbates. a–c Calculated absorption energies as a function of the distance from the Au or Au/graphene surface to **a** Na, **b** K, and **c** H_2O.

electrodes, we investigated the effect of graphene on the absorption energy of various absorbates using density function theory calculations. To mimic the conditions of the brain cerebrospinal fluid (CSF), we tested three representative adsorbates, sodium (Na) and potassium (K) atoms and water molecules (H_2O), abundantly found in the brain. The absorption energy is defined as the energy alteration caused by the solubility of an adsorbate onto the absorbent, indicating the degree of impure contamination of the electrode surface. The absolute value of the absorption energies of the Au surface was relatively larger than that of the Au/graphene surface irrespective of the type of adsorbate (Fig. 2). In other words, the pristine Au surface is likely to be readily affected by various ions or molecules present in the brain, leading to the suppression of electrical conduction between the electrode and the cortical surface. In contrast, the graphene sheet of the Au/graphene electrodes seems to act as a protecting layer to mitigate the deleterious effects.

In vivo experiments of the hybrid graphene electrode array

We performed brain signal recording by placing both the 32-channel hybrid graphene–Au array and Au electrode array on the exposed area ($6 \times 6.2\,mm^2$) of each hemisphere to test the superiority of ECoG measurement with the hybrid graphene electrode over the Au electrode (Fig. 3a). Bicuculline (15×10^{-3} M), which induces ictal- and interictal-like neural activities, was applied to the cortical surface. The hybrid graphene–Au electrode detected brain waves more accurately because of the low noise effect (i.e., high SNR) compared with the Au electrode (Fig. 3b). To clearly compare the noise level and SNR of both electrodes, the interictal-like activities of both electrodes were recorded (Fig. 3c). The measured average root mean square values of the hybrid electrode and the Au electrode were 10.19 ± 1.12 and $93.25 \pm 18.56\,\mu V$, respectively, indicating that the hybrid electrode exhibits a noise value 8–9 times lower than that of the Au electrode. The average SNRs for the hybrid electrode and Au electrode were 51.68 ± 4.45 and 5.66 ± 2.54, respectively. In addition, our hybrid electrode showed an SNR superior to those of reported electrodes such as Au[19,20], Pt[21], PEDOT:PSS[6], and nanostructured carbon[22], except in a few types, including transistors and capacitors (Fig. 3d and Supplementary Fig. 3). Upon the application of bicuculline, ictal-like activity was observed in most of the recorded cortical areas. Notably, the hybrid graphene electrodes with high SNR allow high-resolution ictal-like busting activities (Fig. 3e), yielding a reliable recording of the beta wave, as highlighted in the power spectrum analysis.

To monitor the neural activity at the cortical surface in rats with status epilepticus (SE), we used hybrid graphene–Au electrodes to record the multiscale brain activity (Fig. 4a). After successive administration of pilocarpine, SE states were observed across the following stages: normal state (stage 0), motionless staring and orofacial automatism (stage 1), nodding (stage 2), forelimb clonus (stage 3), rearing and falling (stage 4), and generalized seizures (stage 5) (Fig. 4b). The hybrid graphene electrodes detected different neural response patterns of high-resolution LFPs according to each stage of behavioral change using Racine's scale (Fig. 4c). This result demonstrates the in situ measurement of neural activities at the cortical surface using our hybrid graphene electrode array, which allows concurrent observation of neural activities and behavioral changes.

We investigated whether cortical surface stimulation could reduce hyperexcitable firing and behavioral symptoms of chronic seizures in awake, free-moving animals. Successive intraperitoneal administration of pilocarpine induced hyperexcitable neural activities accompanied by behavioral abnormalities. After recording, the recording graphene electrodes were switched to a stimulating mode. We delivered sinusoidal high-frequency stimulation

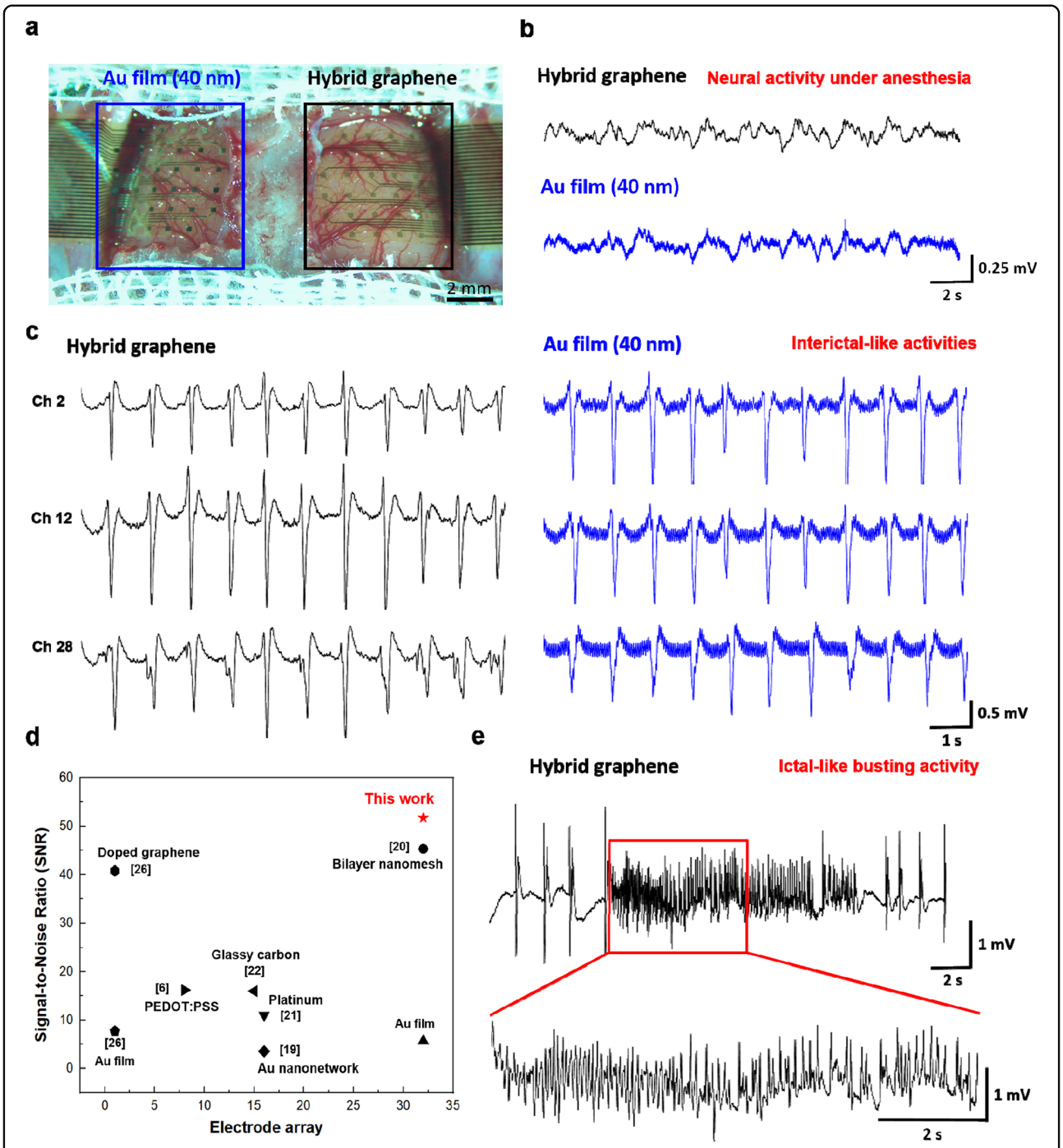

Fig. 3 In vivo multichannel recording of neuronal activities in rats. a Photograph of the 32-ch Au electrode array and hybrid graphene electrode array placed on the somatosensory system. **b** Neural activity under anesthesia. **c** Interictal-like activities recorded by both electrode types placed on the same hemisphere. **d** Comparison of the signal-to-noise ratio (SNR) of the hybrid graphene electrodes with SNRs from electrodes in previous studies. The hybrid electrode shows a higher SNR. **e** Ictal-like busting activity recorded by the hybrid graphene electrode after topical application of bicuculline.

(sHFS; 200 μA, 100 Hz, 1 h) through the same hybrid electrodes. sHFS significantly suppressed the bursting discharges as the wavelength and amplitude of the 0–60 Hz signals were reduced (Fig. 5a, Supplementary Fig. 4, and Supplementary Movie 1). The effects of sHFS on generalized seizures were further analyzed using the behavioral parameters of the Racine scale and electrophysiological parameters of the number and amplitude of

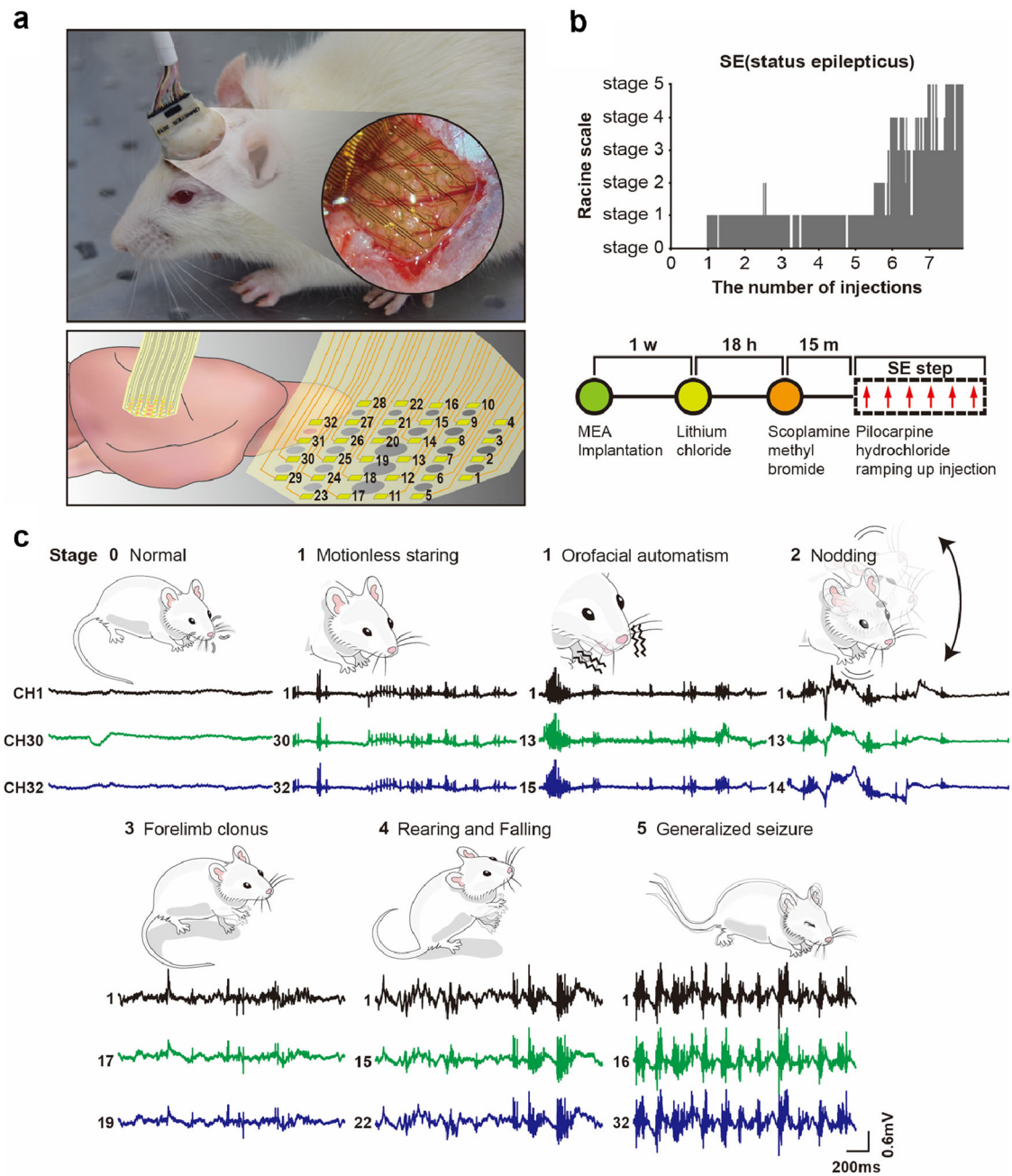

Fig. 4 Recording of SE states in a free-moving rat using a hybrid graphene multichannel electrode. a Photograph (top) and topographical design (bottom) of a hybrid graphene electrode. **b** Behavioral monitoring of SE stages according to Racine's scale after successive injection of 10 mg/kg of pilocarpine every 30 min (top), and a timeline of sequential experiments from hybrid graphene electrode implantation to induction of SE state (bottom). **c** Representative electrocorticograms at each behavior state: normal state (stage 0), motionless staring and orofacial automatism (stage 1), nodding (stage 2), forelimb clonus (stage 3), rearing and falling (stage 4), and generalized seizure (stage 5). The hybrid graphene electrode array allows concurrent observation of neural activities and behavioral changes in awake, free-moving animals.

spikes (Fig. 5b). Following sHFS, stages 4 and 5 were effectively reduced to stages 2 and 3 (Fig. 5b, left). The number of spikes was significantly reduced from 35.40 ± 4.13 to 1.40 ± 0.51 (t test, $t = 8.170$, $p < 0.005$). The amplitude of spikes was reduced from 860.45 ± 3.52 (upward deflection) and -601.03 ± 3.93 (downward deflection) to 202.59 ± 1.61 and -262.86 ± 1.92, respectively ($t_{up} = 170.11$, $p_{up} < 0.005$; $t_{down} = 77.378$, $p_{down} < 0.005$). Theta (4–8 Hz) and alpha (8–13 Hz) rhythms have been widely reported as brain oscillations associated with

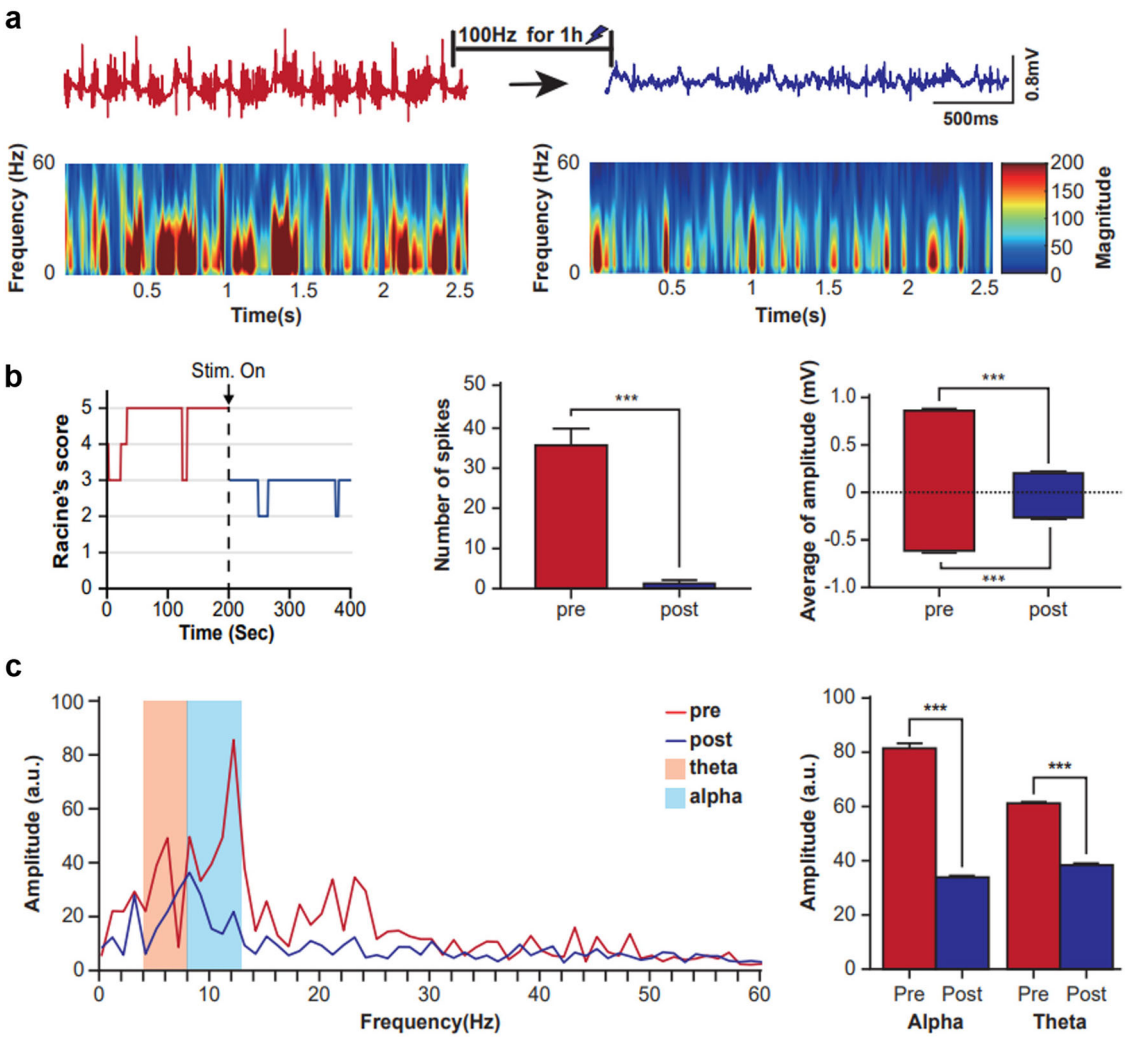

Fig. 5 Therapeutic effects of the hybrid graphene multichannel electrode on epileptic seizures. a Representative traces and spectrograms of generalized seizures (red, before sHFS) and suppression of epileptiform activities (blue, after sHFS). **b** Histograms show that cortical sHFS (200 μA, 100 Hz, 1 h) reduced the behavioral severity and the number and amplitude of spikes in SE rats. **c** Fourier transformation prestimulation (red line) and poststimulation (blue line). Theta and alpha wavelengths are significantly reduced after cortical sHFS. Data are expressed as the mean ± standard error (SEM). ***$p < 0.001$.

the generation and propagation of epileptiform discharges[23]. The increased alpha and theta oscillations under epileptic seizures were significantly reduced after sHFS from 40.44 ± 0.87 (alpha) and 30.59 ± 0.22 (theta) to 16.89 ± 0.12 and 19.27 ± 0.23, respectively (Fig. 5c; $t_{alpha} = 26.691$, $p_{alpha} < 0.005$; $t_{theta} = 35.138$, $p_{theta} < 0.005$). These results showed that the hybrid graphene–Au electrode successfully differentiates epileptic discharges from normal brain signals, and delivery of sHFS via the hybrid electrodes corrects the pilocarpine-induced epileptiform discharges and abnormal behaviors in awake, free-moving animals.

We examined whether 40 days of long-term implantation of hybrid graphene electronics in the cortex guarantees safety. To test biocompatibility, we performed immunohistochemistry using two major cell types of the brain: neurons and glia. No difference was observed in the number of neurons between the implanted and control hemispheres of the awake animals when NeuN, a neuronal molecular marker, was used (Fig. 6a, $t = 0.108$, $p = 0.915$, $n = 12$). Similarly, glial protein and GFAP expression did not change after implantation (Fig. 6b, $t = 0.913$, $p = 0.370$, $n = 14$). These results demonstrate that our hybrid electrodes are biocompatible over the long term.

Discussion

Conventional materials for the diagnosis and treatment of central nervous system (CNS) disorders face a number of limitations, which motivate the establishment of new

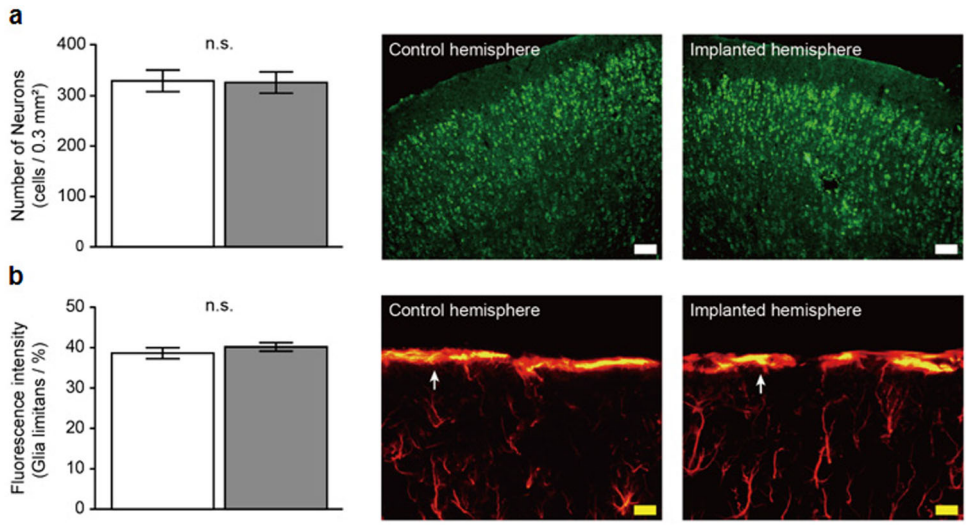

Fig. 6 Immunohistochemistry data for the biocompatibility of the hybrid graphene multichannel electrode. a No difference was observed in the number of neurons (labeled with NeuN, a neuronal molecular marker) between implanted (gray) and control (white) hemispheres of awake animals (scale bar = 100 μm). **b** No difference was observed in the number of glia (labeled with GFAP, a glia molecular marker) between implanted (gray) and control (white) hemispheres of the awake animals (scale bar = 20 μm). The arrows indicate glia limitans, the index for brain inflammation. Data are expressed as the mean ± SEM. n.s. not significant.

tools to surpass currently limited technologies in neurodiagnostics and neurotherapeutics[24]. To overcome the existing drawbacks, such as spatiotemporal resolution, clinical inadaptability, nonselective effects, and material toxicity, neuroscientists have started exploring the diagnostic and therapeutic usage of nanomaterials in various brain disorders, such as Parkinson's disease (PD)[25,26], Alzheimer's disease (AD)[27–30], epilepsy[31], gliom[32], stroke[33], and hearing loss-induced tinnitus[34]. Nanomaterials with high conductivity and chemical compatibility also need to possess high conductivity, biocompatibility, and superior tunability of their properties by varying crystallite size and shape. Silicon, gold, and graphene are nanomaterials that fulfill these requirements and are widely used in brain research [35–38]. Silicon is electrically conductive and easily modifiable into the nontoxic silicic membrane. In addition, porous formation allows high accessibility of drug loadings, being one of the materials widely used in nanotechnology[39]. However, silicon is impeded by low thermal stability and inferior irreversible capacity[40]. Gold, another alternative nanomaterial, shows high thermal stability and superior irreversible capacity, demonstrating a promising outcome in nanotechnology specific to neurodegenerative disease treatment[37]. Additionally, gold nanoparticles are easily conjugated with designed drugs through a chemisorption process, enabling gold nanoparticles to be used to recognize an AD toxic protein, the β-amyloid aggregate, and release drugs at a target site[41]. However, there are a few caveats for clinical use. Gold remains toxic and unstable in the body when applied for drug delivery [42,43]. In these regards, graphene, which is comparable to silicon and gold and can replace them, has shown great promise for application in diagnostic and therapeutic methods[44].

Neurostimulation has become an integral part of the clinical diagnosis and treatment of neurological conditions. Traditional neurostimulation methods, such as deep brain stimulation, vagus nerve stimulation, responsive neurostimulation (RNS), and repetitive transcranial magnetic stimulation, are clinically beneficial for repetitive measurements. However, their therapeutic outcomes are not conclusive because of poor spatiotemporal resolution of recordings and nonspecific stimulation. Recent studies with hybrid graphene materials are highly compatible with several advanced biomedical systems, such as neuroimaging, neuroregeneration, optogenetics, and functional neurosurgery[33,45,46]. There are encouraging results showing that graphene electrodes can be successfully applied to various brain disorders for diagnostic and therapeutic purposes. In particular, hybrid graphene-based electrodes exhibit long-term biocompatibility and mechanical flexibility, thereby providing stable recordings from the convoluted surface of the mammalian brain. More importantly, they allow large-scale real-time recording[47,48].

Epilepsy is an intractable chronic disorder with characteristic repeated convulsions that stem from abnormally excessive activities of damaged brain areas, in particular the temporal lobe of the cerebral cortex[31,49,50]. Epilepsy is often accompanied by psychological symptoms such as anxiety, depression, memory impairment, and suicidal

thoughts[51–54]. Excessive excitation (*E*) surpassing inhibition (*I*) (i.e., imbalanced *E*/*I* ratio) in neural networks leads to the loss of cognition and frequent involuntary movement[55–57]. Recently, a graphene electrode array was used to suppress epileptic seizures in a rodent model[31]. The graphene multichannel electrode was placed into a cortical area to detect epileptiform discharges and sequentially apply electrical stimulations embedded in a subset of the graphene multichannel array to eliminate abnormal brain discharges[31,58,59]. The graphene electrode array shows more promising therapeutic outcomes, such as minimal physical damage, negligible immunoreactivity, superior biocompatibility, high spatiotemporal resolution, and superior electrical conductivity[60,61].

Although previous studies have shown the therapeutic effects of high-frequency stimulation on epileptiform activity[31], the neural mechanism underlying the suppression of epileptic discharge and behavior by cortical stimulation remains unclear. The cortical surface has cross-columnar interactions along the horizontal and columnar axonal projections. In addition, the dendrites in the apical tuft of the cortical pyramidal neurons have long horizontal projections and integrate heterogeneous inputs over other cortical areas[62,63]. Such axonal and dendritic network complexity is likely involved in the generation and/or propagation of epileptic discharges. The rhythmic pattern of seizures can interfere with high-frequency stimulation, presumably due to the depolarization block of action potentials and desynchronization of brain waves, thereby leading to synaptic inhibition across vertical and horizontal connections in the cortex. In addition, neuromodulatory afferents on the cortical surface can be part of the neural mechanisms underlying the suppression of seizure activity. Some neuromodulators mediate dramatic changes in the amplitude and selectivity of cortical responses[64]. For example, cortical activation of cholinergic and dopaminergic synapses alters the firing rates and patterns of cells and can modulate cortical responses[65–68]. This neuromodulatory innervation can induce synaptic plasticity in the cortex[68–72]. Because neuromodulatory afferents may be concentrated in the apical dendrites of the cortical surface, our studies support the central role of neuromodulators in the suppression of epileptic discharges and behaviors.

Experimental methods

Fabrication of the hybrid graphene multichannel electrode array

A PI film with 2–4 μm thickness was formed on a glass substrate using a liquid PI precursor (Sigma–Aldrich). Cr/Au (3 nm/40 nm) was deposited on the PI substrate patterned using photolithography to create contact pads after the etching process to form the thru-holes of the PI substrate. After transferring monolayer graphene synthesized via the CVD method into the electrode pattern, a 6-nm-thick Au layer was deposited on the graphene layer. Then, another monolayer of graphene was stacked on it using a polymethyl methacrylate supporting layer. Subsequently, oxygen plasma etching (40 sccm, 100 W, 10 s) was performed, and the electrode was immersed in the electrode pattern for 1–2 s in the gold etching solution. The oxygen plasma etching process was repeated. Finally, a thin SU-8 (2 μm) layer was spin-coated and patterned for encapsulation, covering almost all parts except the electrode and FPC connection areas.

Electrochemical characterization

The electrode impedance and CV values were measured using an electrochemical workstation (ZIVE SP1). Impedance measurement involved a frequency sweep from 1 Hz to 100 kHz with an Ag/AgCl reference electrode and platinum wire counter electrode in 0.01 M PBS solution, and CV was performed three times between −1 V and 1 V versus the Ag/AgCl reference electrode in PBS solution at a scan rate of 200 mV s^{-1} A. The total charge transfer capacity was calculated by integrating the time over the entire CV curve.

In vivo animal surgery

All animal handling procedures were approved by the Institutional Animal Care and Use Committee of Gbrain Inc. (GB-IACUC-20R08001) and Incheon National University (INU-ANIM-2017-08). Sprague–Dawley (SD) rats acquired from Charles River Laboratories were housed under standard laboratory conditions [22 °C, 55%, 12-h light/dark cycle (light on: 6:00 h; light off: 18:00 h, ad libitum)]. Eight-week-old rats were anesthetized with ketamine (80 mg/kg) and xylazine (7 mg/kg) by intraperitoneal injection, or anesthesia was induced by placing the rats in an anesthesia induction chamber (22 × 15 × 15 cm) containing 3% isoflurane (Hana Pharm. Co., Ltd., Seoul, Korea) with N_2O and O_2 for 10 min. Subsequently, anesthesia was maintained using 2% isoflurane inhalation, and the animals' body temperature (36.5 °C) and anesthesia state (respiratory rate, heart rate, corneal reflex, and hind paw reflex) were continuously monitored throughout the experiment. CSF was drained to reduce the probability of cerebral edema. During this procedure, the muscles were bluntly dissected over the occipital skull to expose the cisterna magna above the axis at the top of the spinal cord. The dura was slit, and CSF was drained using soft cotton; then, the skull was opened (4 × 4 mm) using a surgical blade. Subsequently, the hybrid graphene electrodes were implanted subdurally.

Induction of status epilepticus

To induce SE in rats, lithium chloride (127 mg/kg; Sigma–Aldrich, Saint-Louis, MO) was administered via intraperitoneal injection. After 18–24 h, scopolamine

methyl bromide was administered (1 mg/kg; Sigma–Aldrich). Pilocarpine, a muscarinic agonist (10 mg/kg; Sigma–Aldrich), was dissolved in saline and repeatedly administered intraperitoneally every 30 min to induce continuous seizures, based on the Racine scale. Diazepam (10 mg/kg; Samjin Pharm. Co., Ltd., Hwasung, Korea) and pentobarbital sodium (25 mg/kg; Hanlim Pharm. Co., Ltd., Seoul, Korea) were administered to the rats with SE for 90 min to reduce the level of hippocampal damage.

Brain recording and stimulation of awake animals

The brain activity of animals under normal and SE states was monitored using the Intan RHS Stim/Recording System (Intan Technologies, Los Angeles, CA, USA). The hybrid graphene electrodes were connected to a flexible printed circuit board, a hard printed circuit board (to produce a headstage) customized for long-term implantation, and an RHS interface board. Behavior and brain rhythms were simultaneously monitored in real time. Neural activity was analyzed using MATLAB (R2020b, MathWorks, Natick, MA, USA). Cortical stimulation (200 μA, 100 Hz, 1 h) was delivered through a hybrid graphene electrode array connected to the RHS interface board.

Tissue preparation and histology

Forty days after the implantation of a hybrid graphene–Au array, the rats were perfused transcardially with PBS, followed by 4% paraformaldehyde in PBS (T&I Biotechnology, Seoul, Korea). Their brains were isolated from the skull, postfixed in 4% paraformaldehyde for 24 h, and then placed in a graded sucrose solution (15% and 30% in sequence; prepared in PBS) at 4 °C. The brain samples were frozen at 80 °C before sectioning. Frozen sections of 20-μm thickness were obtained using a cryostat microtome (Leica CM1520, Leica Biosystems, Wetzlar, Germany). The tissue sections were dried at 60 °C for 2 h, washed with 0.3% Triton X-100 prepared in PBS (PBST; Sigma–Aldrich), and placed in a blocking solution consisting of 3% normal goat serum (Jackson ImmunoResearch Inc., West Grove, PA, USA) in PBST for 1 h. The slices were incubated with the following primary antibody solutions overnight at 4 °C: anti-glial fibrillary acidic protein (anti-GFAP; 1:500, monoclonal mouse IgG1 conjugated to Cy3; Sigma–Aldrich) for astrocyte staining and anti-NeuN (1:500, polyclonal rabbit IgG; Invitrogen, Carlsbad, CA) for neuron staining. Secondary antibodies were diluted at a 1:500 ratio and included FITC-conjugated goat anti-rabbit IgG (Abcam, Cambridge, UK) for NeuN. The tissue sections were mounted with an aqueous mounting medium containing 4-6-diaminido-2-phenylindole (Vector Laboratories, Inc., Burlingame, CA, USA). The final samples were visualized under an Axioplan2 imaging microscope (Zeiss, Oberkochen, Germany). The fluorescence intensity measurement of GFAP and counting of NeuN-positive cells were performed using ImageJ software (http://rsb.info.nih.gov/ij/).

Statistical analysis

To determine the therapeutic effect of cortical stimulation, all electrophysiological data obtained before and after stimulation were compared using a paired Student's t test. Data analysis of the spectrogram and fast Fourier transform was performed using MATLAB (R2020b, MathWorks). An unpaired t test was used to compare the differences between the implanted and control hemispheres and assess the safety of hybrid graphene electrodes. All statistical analyses and graph preparations were performed using RStudio (version 1.3.1073; RStudio, Inc., Boston, MA, USA).

Acknowledgements

This work was supported by the Technology Innovation Program (20012355, Fully implantable closed loop Brain to X for voice communication) funded by MOTIE, Korea and High Risk, High Return Research Program (2020) in the Incheon National University to S.Y. and the National Research Foundation of Korea (NRF-2015R1A3A2066337) to J.-H.A. S.Y. acknowledges grants from the Research Grants Council of Hong Kong (11101922 and 11102618).

Author details

[1]School of Electrical & Electronic Engineering, Yonsei University, Seoul 03722, Republic of Korea. [2]Department of Nano-bioengineering, Incheon National University, Incheon 22012, Republic of Korea. [3]Gbrain Inc., Incheon, Republic of Korea. [4]Department of Physics, Incheon National University, Incheon 22012, Republic of Korea. [5]Department of Neuroscience, City University of Hong Kong, Tat Chee Avenue, Kowloon, Hong Kong

Author contributions

J.-H.A., S.C.Y., and S.G.Y. planned and supervised the project. J.L. conducted most of the experiments regarding the fabrication and electrochemical characterization of devices. S.L., S.L., and K.K. performed the animal experiments and neural recording and stimulation for freely moving rats. J.K. supported the experiments. J.H. and J.K. conducted theoretical calculations. All authors contributed to writing the manuscript.

Data availability

The data that support the plots within this paper and other findings of this study are available from the corresponding authors upon reasonable request.

Competing interests

The authors declare no competing interests.

Supplementary information The online version contains supplementary material available at https://doi.org/10.1038/s41427-023-00464-1.

Received: 13 October 2022 Revised: 10 January 2023 Accepted: 11 January 2023.
Published online: 17 February 2023

References

1. Marescaux, C., Vergnes, M. & Depaulis, A. Genetic absence epilepsy in rats from Strasbourg — a review. *J. Neural Transm. Suppl.* **35**, 37–69 (1992).
2. Gutnick, M. J. & Prince, D. A. Thalamocortical relay neurons: antidromic invasion of spikes from a cortical epileptogenic focus. *Science* **176**, 424–426 (1972).

3. Kringelbach, M. L., Jenkinson, N., Owen, S. L. & Aziz, T. Z. Translational principles of deep brain stimulation. *Nat. Rev. Neurosci.* **8**, 623–635 (2007).
4. Theodore, W. H. & Fisher, R. S. Brain stimulation for epilepsy. *Lancet Neurol.* **3**, 111–118 (2004).
5. Rush, A. J. et al. Vagus nerve stimulation (VNS) for treatment-resistant depressions: a multicenter study. *Biol. Psychiatry* **47**, 276–286 (2000).
6. Khodagholy, D. et al. In vivo recordings of brain activity using organic transistors. *Nat. Commun.* **4**, 1575 (2013).
7. Khodagholy, D. et al. NeuroGrid: recording action potentials from the surface of the brain. *Nat. Neurosci.* **18**, 310–315 (2015).
8. Kim, D. H. et al. Dissolvable films of silk fibroin for ultrathin conformal bio-integrated electronics. *Nat. Mater.* **9**, 511–517 (2010).
9. Yu, K. J. et al. Bioresorbable silicon electronics for transient spatiotemporal mapping of electrical activity from the cerebral cortex. *Nat. Mater.* **15**, 782–791 (2016).
10. Viventi, J. et al. Flexible, foldable, actively multiplexed, high-density electrode array for mapping brain activity in vivo. *Nat. Neurosci.* **14**, 1599–1605 (2011).
11. Escabí, M. A. et al. A high-density, high-channel count, multiplexed μECoG array for auditory-cortex recordings. *J. Neurophysiol.* **112**, 1566–1583 (2014).
12. Kostarelos, K., Vincent, M., Hebert, C. & Garrido, J. A. Graphene in the design and engineering of next-generation neural interfaces. *Adv. Mater.* **29**, 1700909 (2017).
13. Li, N. et al. The promotion of neurite sprouting and outgrowth of mouse hippocampal cells in culture by graphene substrates. *Biomaterials* **32**, 9374–9382 (2011).
14. Sahni, D. et al. Biocompatibility of pristine graphene for neuronal interface: laboratory investigation. *J. Neurosurg.* **11**, 575–583 (2013).
15. Geim, A. K. & Novoselov, K. S. The rise of graphene. *Nat. Mater.* **6**, 183–191 (2007).
16. Cheng, Z., Li, Q., Li, Z., Zhou, Q. & Fang, Y. Suspended graphene sensors with improved signal and reduced noise. *Nano Lett.* **10**, 1864–1868 (2010).
17. Schedin, F. et al. Detection of individual gas molecules adsorbed on graphene. *Nat. Mater.* **6**, 652–655 (2007).
18. Merrill, D. R., Bikson, M. & Jefferys, J. G. R. Electrical stimulation of excitable tissue: design of efficacious and safe protocols. *J. Neurosci. Methods* **141**, 171–198 (2005).
19. Seo, J. W. et al. Artifact-free 2D mapping of neural activity in vivo through transparent gold nanonetwork array. *Adv. Funct. Mater.* **30**, 2000896 (2020).
20. Qiang, Y. et al. Transparent arrays of bilayer-nanomesh microelectrodes for simultaneous electrophysiology and two-photon imaging in the brain. *Sci. Adv.* **4**, eaat0626 (2018).
21. Pazzini, L. et al. An ultra-compact integrated system for brain activity recording and stimulation validated over cortical slow oscillations in vivo and in vitro. *Sci. Rep.* **8**, 16717 (2018).
22. Nimbalkar, S. et al. Ultra-capacitive carbon neural probe allows simultaneous long-term electrical stimulations and high-resolution neurotransmitter detection. *Sci. Rep.* **8**, 6958 (2018).
23. Buzsaki, G. & Draguhn, A. Neuronal oscillations in cortical networks. *Science* **304**, 1926–1929 (2004).
24. Baldrighi, M., Trusel, M., Tonini, R. & Giordani, S. Carbon nanomaterials interfacing with neurons: an in vivo perspective. *Front. Neurosci.* **10**, 250 (2016).
25. Kim, D. et al. Graphene quantum dots prevent α-synucleinopathy in Parkinson's disease. *Nat. Nanotechnol.* **13**, 812–818 (2018).
26. Xiong, S. et al. Targeted graphene oxide for drug delivery as a therapeutic nanoplatform against Parkinson's disease. *Biomater. Sci.* **9**, 1705–1715 (2021).
27. Liu, C. & Luo, X. Potential molecular and graphene oxide chelators to dissolve amyloid-β plaques in Alzheimer's disease: a density functional theory study. *J. Mater. Chem. B* **9**, 2736–2746 (2021).
28. Liu, Y. et al. Graphene quantum dots for the inhibition of β amyloid aggregation. *Nanoscale* **7**, 19060–19065 (2015).
29. Murphy, M. P. & LeVine, H. 3rd Alzheimer's disease and the amyloid-beta peptide. *J. Alzheimers Dis.* **19**, 311–323 (2010).
30. Tak, K., Sharma, R., Dave, V., Jain, S. & Sharma, S. *Clitoria ternatea* mediated synthesis of graphene quantum dots for the treatment of Alzheimer's disease. *ACS Chem. Neurosci.* **11**, 3741–3748 (2020).
31. Park, S.-W. et al. Epidural electrotherapy for epilepsy. *Small* **14**, 1801732 (2018).
32. Lu, Y. J. et al. Improving thermal stability and efficacy of BCNU in treating glioma cells using PAA-functionalized graphene oxide. *Int. J. Nanomed.* **7**, 1737–1747 (2012).
33. Liu, T. C. et al. Implantable graphene-based neural electrode interfaces for electrophysiology and neurochemistry in in vivo hyperacute stroke model. *ACS Appl. Mater. Interfaces* **8**, 187–196 (2016).
34. Lee, M. et al. Graphene-electrode array for brain map remodeling of the cortical surface. *NPG Asia Mater.* **13**, 65 (2021).
35. Betty, C. A. Porous silicon: a resourceful material for nanotechnology. *Recent Pat. Nanotechnol.* **2**, 128–136 (2008).
36. Tu, L., Luo, Z., Wu, Y. L., Huo, S. & Liang, X. J. Gold-based nanomaterials for the treatment of brain cancer. *Cancer Biol. Med.* **18**, 372–387 (2021).
37. Prades, R. et al. Delivery of gold nanoparticles to the brain by conjugation with a peptide that recognizes the transferrin receptor. *Biomaterials* **33**, 7194–7205 (2012).
38. Bramini, M. et al. Interfacing graphene-based materials with neural cells. *Front. Syst. Neurosci.* **12**, 12 (2018).
39. McInnes, S. J. & Voelcker, N. H. Silicon-polymer hybrid materials for drug delivery. *Future Med. Chem.* **1**, 1051–1074 (2009).
40. Zhao, X. & Lehto, V.-P. Challenges and prospects of nanosized silicon anodes in lithium-ion batteries. *Nanotechnology* **32**, 042002 (2020).
41. Kogan, M. J. et al. Nanoparticle-mediated local and remote manipulation of protein aggregation. *Nano Lett.* **6**, 110–115 (2006).
42. Zhang, X. D. et al. Toxicologic effects of gold nanoparticles in vivo by different administration routes. *Int. J. Nanomed.* **5**, 771–781 (2010).
43. Arvizo, R., Bhattacharya, R. & Mukherjee, P. Gold nanoparticles: opportunities and challenges in nanomedicine. *Expert Opin. Drug Deliv.* **7**, 753–763 (2010).
44. Dasari Shareena, T. P., McShan, D., Dasmahapatra, A. K. & Tchounwou, P. B. A review on graphene-based nanomaterials in biomedical applications and risks in environment and health. *Nanomicro Lett.* **10**, 53 (2018).
45. Mattei, T. A. & Rehman, A. A. Technological developments and future perspectives on graphene-based metamaterials: a primer for neurosurgeons. *Neurosurgery* **74**, 499–516 (2014); discussion 516.
46. Thunemann, M. et al. Deep 2-photon imaging and artifact-free optogenetics through transparent graphene microelectrode arrays. *Nat. Commun.* **9**, 2035 (2018).
47. Masvidal-Codina, E. et al. High-resolution mapping of infraslow cortical brain activity enabled by graphene microtransistors. *Nat. Mater.* **18**, 280–288 (2019).
48. Blaschke, B. M. et al. Mapping brain activity with flexible graphene microtransistors. *2D Mater.* **4**, 025040 (2017).
49. Sirven, J. I. Epilepsy: a spectrum disorder. *Cold Spring Harb. Perspect. Med.* **5**, a022848–a022848 (2015).
50. Choi, G., Kang, H., Chu, W., Yang, S. & Yang, S. Dynamics of longitudinal dentate gyrus axons associated with seizure. *J. Physiol.* **599**, 2273–2281 (2021).
51. Kuroda, N. Mental health considerations for patients with epilepsy during COVID-19 crisis. *Epilepsy Behav.* **111**, 107198–107198 (2020).
52. Berkovic, S. F., Mulley, J. C., Scheffer, I. E. & Petrou, S. Human epilepsies: interaction of genetic and acquired factors. *Trends Neurosci.* **29**, 391–397 (2006).
53. Engel, J. Mesial temporal lobe epilepsy: what have we learned? *Neuroscientist* **7**, 340–352 (2001).
54. Vadlamudi, L., Scheffer, I. E. & Berkovic, S. F. Genetics of temporal lobe epilepsy. *J. Neurol. Neurosurg. Psychiatry* **74**, 1359 (2003).
55. Yang, S. & Cox, C. L. Excitatory and anti-oscillatory actions of nitric oxide in thalamus. *J. Physiol.* **586**, 3617–3628 (2008).
56. Stafstrom, C. E. Epilepsy: a review of selected clinical syndromes and advances in basic science. *J. Cereb. Blood Flow. Metab.* **26**, 983–1004 (2006).
57. Noh, W., Pak, S., Choi, G., Yang, S. & Yang, S. Transient potassium channels: therapeutic targets for brain disorders. *Front. Cell. Neurosci.* **13**, 265 (2019).
58. Bae, S. et al. Roll-to-roll production of 30-inch graphene films for transparent electrodes. *Nat. Nanotechnol.* **5**, 574–578 (2010).
59. Nolan, S. J., Marson, A. G., Weston, J. & Tudur Smith, C. Phenytoin versus valproate monotherapy for partial onset seizures and generalised onset tonic-clonic seizures: an individual participant data review. *Cochrane Database Syst. Rev.* **4**, Cd001769 (2016).
60. Calia, A. B. et al. Full bandwidth electrophysiology of seizures and epileptiform activity enabled by flexible graphene micro-transistor depth neural probes. *Nat. Nanotechnol.* **17**, 301–309 (2021).
61. Gulino, M., Kim, D., Pané, S., Santos, S. D. & Pêgo, A. P. Tissue response to neural implants: the use of model systems toward new design solutions of implantable microelectrodes. *Front. Neurosci.* **13**, 689 (2019).
62. Brown, S. P. & Hestrin, S. Intracortical circuits of pyramidal neurons reflect their long-range axonal targets. *Nature* **457**, 1133–1136 (2009).

63. Spruston, N. Pyramidal neurons: dendritic structure and synaptic integration. *Nat. Rev. Neurosci.* **9**, 206–221 (2008).
64. Schulze-Bonhage, A. Brain stimulation as a neuromodulatory epilepsy therapy. *Seizure* **44**, 169–175 (2017).
65. Kilgard, M. P. & Merzenich, M. M. Cortical map reorganization enabled by nucleus basalis activity. *Science* **279**, 1714–1718 (1998).
66. Froemke, R. C., Merzenich, M. M. & Schreiner, C. E. A synaptic memory trace for cortical receptive field plasticity. *Nature* **450**, 425–429 (2007).
67. Bao, S., Chan, V. T. & Merzenich, M. M. Cortical remodelling induced by activity of ventral tegmental dopamine neurons. *Nature* **412**, 79–83 (2001).
68. Froemke, R. C. Plasticity of cortical excitatory-inhibitory balance. *Annu. Rev. Neurosci.* **38**, 195–219 (2015).
69. Buonomano, D. V. & Merzenich, M. M. Cortical plasticity: from synapses to maps. *Annu. Rev. Neurosci.* **21**, 149–186 (1998).
70. Weinberger, N. M. Specific long-term memory traces in primary auditory cortex. *Nat. Rev. Neurosci.* **5**, 279–290 (2004).
71. Malenka, R. C. & Bear, M. F. LTP and LTD: an embarrassment of riches. *Neuron* **44**, 5–21 (2004).
72. Blundon, J. A. & Zakharenko, S. S. Presynaptic gating of postsynaptic synaptic plasticity: a plasticity filter in the adult auditory cortex. *Neuroscientist* **19**, 465–478 (2013).